Feb 7 2021

Radiation Absorption Lab

David Freifeld, Zachary Sayyah

Purpose: To quantify the absorption capability of various common materials in respect to multiple types of radiation emitted from different objects as well as determine the type of radiation emitted from these objects.

Materials:

- Vernier Geiger counter
- LabQuest Mini (and associated cables)
- Facial tissues
- Aluminum plates (0.02 in, 0.025 in, 0.032 in, 0.04 in, 0.05 in, 0.063 in, 0.08 in, 0.09 in, 0.1 in, 0.125 in)
- Lead plates (0.032 in, 0.064 in, 0.125 in, 0.25 in), plastic plates (0.004 in, 0.008 in, 0.03 in, 0.04in)
- Ring stand with clamp
- Fiestaware cup
- Orange pellets
- Yellow pellets
- Green pellets
- Logger Pro.

Procedure:

- Place the Vernier Geiger counter on the ring stand so it is mounted on the clamp.
- Plug the Vernier Geiger counter into the lab quest mini and lab quest mini into the computer.
- Place all radioactive material/pellets at least 3 meters away from the setup.
- Record background radiation for 300 seconds using Logger Pro.
- For all combinations of radioactive source and absorber place source on stand, record at least 1000 counts using logger pro, and repeat this process.

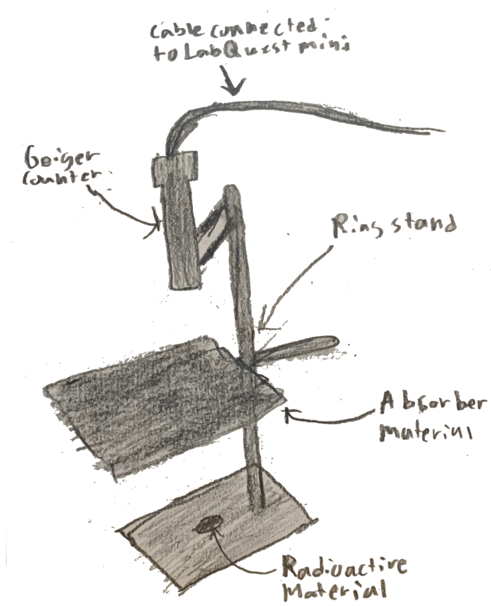

Diagram 1 (right): Illustrated representation of lab setup.

Data:

In order to determine the absorption capability of each material in respect to the various types of unidentified radiation, different thicknesses of such absorbers were used with each type of radioactive pellet. The penetrating radiation for each was recorded.

Absorber Width	Seconds	Counts
0	400	4358
0.032	400	4017
0.064	400	3872
0.125	400	3673
0.25	400	2956

Table 1: A representative sample of the collected data (more specifically the data collected for the Lead-Orange pair).

Additionally, for each setup background radiation was recorded, so that it later could be used to obtain the Adjusted CPS which excludes the varying and irrelevant background radiation.

Seconds	Counts
300	39

Table 2: Background radiation data associated with data in Table 1.

Analysis:

Width	Counts	Seconds	CPS	CPS σ	True CPS	True CPS σ	Adjusted CPS	Adjusted CPS σ	NCR	NCR σ
0	4358	400	10.895	0.165	10.929	0.1656	10.799	0.1669	1	0.0219
0.032	4017	400	10.0425	0.1584	10.0714	0.1589	9.9414	0.1603	0.9206	0.0223
0.064	3872	400	9.68	0.1556	9.7068	0.156	9.5768	0.1574	0.8868	0.0226
0.125	3673	400	9.1825	0.1515	9.2067	0.1519	9.0766	0.1533	0.8405	0.0229
0.25	2956	400	7.39	0.1359	7.4056	0.1362	7.2756	0.1378	0.6737	0.0244

Table 3: Sample of adjustments and calculations performed on recorded data (in this case the same data as in Table 1)

A series of calculations and corrections were required to determine the NCR of each pairing. A dead-time correction, $\frac{x}{(1-(\frac{x}{3500})}$, was used to account for the dead time in the Geiger counter's measurements (yielding the True CPS value seen in the table). The CPS of the background measurement was then subtracted to account for the effects of any background radiation (yielding the Adjusted CPS value in Table 3). Finally, each value was divided by the corrected CPS of the trial without an absorber to yield the Normalized Count Rate (or NCR) to provide an indication of the 'relative intensity' of the remaining radiation. The CPS uncertainty was determined by taking the square-root of the counts (as this yields the variance of the distribution created by the radiation source) divided by the amount of seconds. Standard error propagation formulas for multiplication/division and constant division were then used to determine the associated error with each True CPS, Adjusted CPS, and NCR value.

The NCR and NCR uncertainties for each absorber-source pairing was inputted into a custom Python script to determine the pairing's half-thickness, T. This was done by beginning with an arbitrary initial guess for T, using the relative intensity formula $0.5^{\frac{t}{T}}$ to generate fitted NCR values for each data point. Pearson's s-statistic was then calculated for this fit with $S = \sum \frac{A_i - y_i}{\sigma_i}^2$, where A_i is the fit's approximated NCR value, y_i is the recorded NCR value, and σ_i is the recorded NCR uncertainty. The quality of the fit was then improved by passing our programmatic implementation of Pearson's s-statistic to the minimization function implemented in SciPy (a Python scientific computing library).

Margon, Lampton, and Bowyer's 1976 paper on parameter estimation in X-ray astronomy provides a means for the quantification of uncertainties in these fits in the form of the χ^2 factor. The χ^2 factor yields the maximum S value. Since there is one degree of freedom (T), and desired significance is 0.01 (in order to be below 0.05), the paper defines the χ^2 value to be 6.63.

Numerous calculations were then required in order to obtain the fitted error. Firstly, the χ^2 value 6.63 and S_{min} (where S_{min} is the programmatically determined minimum S statistic) were added yielding an intermediate value. This intermediate value was then subtracted from the function translating it downwards by $6.63 + S_{min}$. The roots were then taken of this new function via a bisection method also implemented in SciPy yielding the upper and lower bounds, where the bounds are the values with an S-statistic of $S_L = S_{min} + \chi^2$.

The resulting fit, fitted error, and previously calculated NCR error were used to generate the following figure utilizing matplotlib (a python graphing utility) and LaTeX.

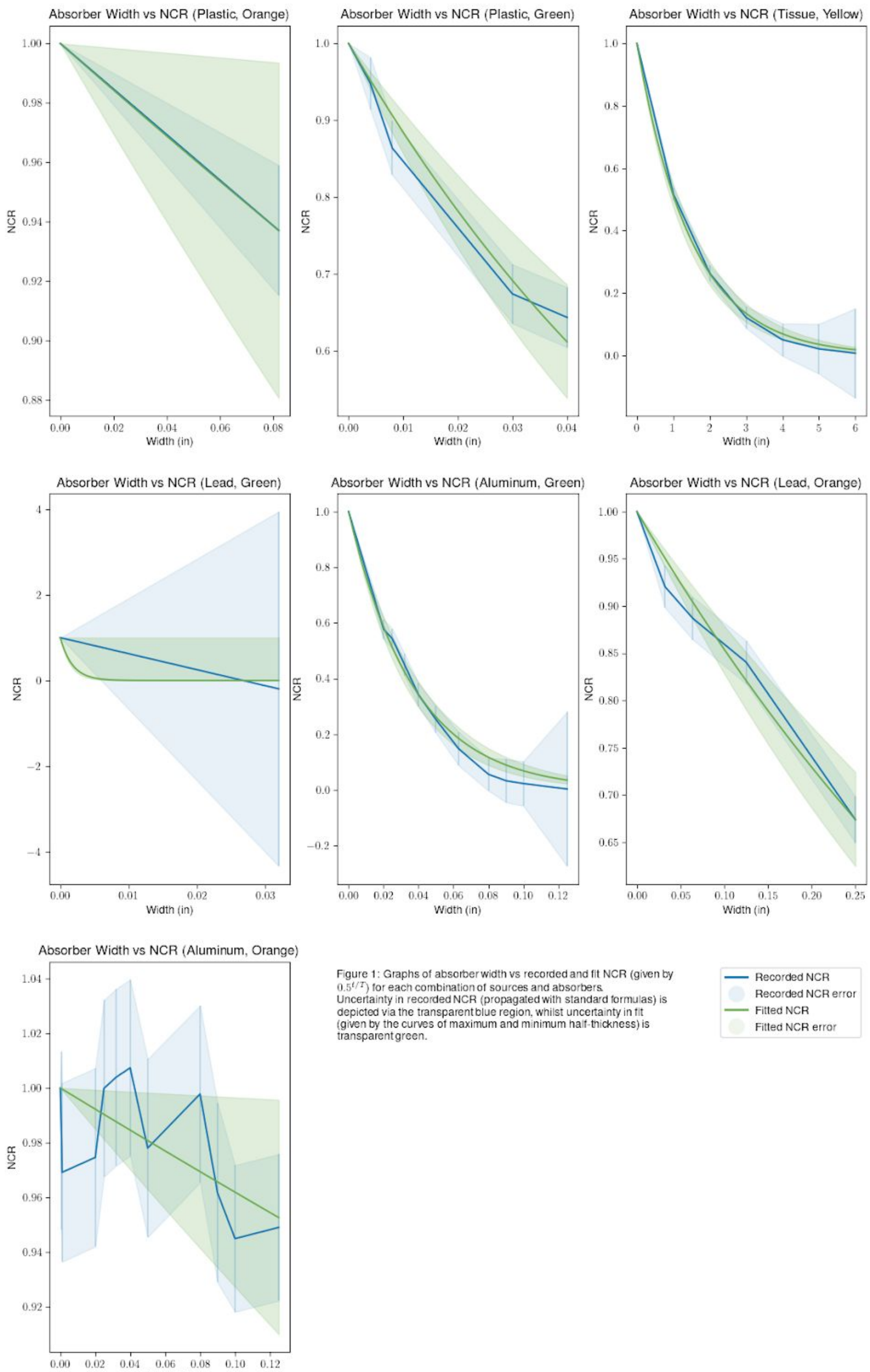

Figure 1: Graphs of absorber width vs recorded and fit NCR (given by $0.5^{t/T}$) for each combination of sources and absorbers.
Uncertainty in recorded NCR (propagated with standard formulas) is depicted via the transparent blue region, whilst uncertainty in fit (given by the curves of maximum and minimum half-thickness) is transparent green.

Material	T_{best}	T_{min}	T_{max}	S_{min}	N-1
Plastic Orange	0.8736	0.4466	8.7385	0	1
Plastic Green	0.0564	0.0448	0.0737	2.356	4
Tissue Yellow	1.0371	0.9314	1.1536	0.3733	6
Lead Green	0.0012	0	10000000	0.0022	1
Aluminum Green	0.0259	0.0229	0.0292	3.5908	10
Lead Orange	0.4391	0.368	0.5369	3.129	4
Aluminum Orange	1.7843	0.918	19.9563	3.5532	11

Table 4: Maximum, minimum, and best half-thicknesses alongside associated S_{min} and N-1 for each combination of absorber and source. Half-thickness is measured in inches (with the notable exception of Tissue Yellow where it is measured in tissues).

Lead was especially absorbent: for both the green and orange radiation sources it had the lowest half-thickness out of all three absorbers. This result was expected as lead is widely used in radiation shielding applications due to its high density (allowing it to scatter and stop alpha, beta, and gamma radiation).

However, a more noticeable quality of the lead data is the very large uncertainty associated with the Lead-Green pairing, which is also visible through the abnormal uncertainty region for Lead-Green's graph in Figure 1. This is entirely caused by the limitations of the data analysis program, with the T_{max} of 10^7 being entirely arbitrary. As was described earlier, to find these bounds, the program shifts the curve down by $S_{min} + \chi^2$ and attempts to use the bisection method to find the roots of the shifted curve (and by extension the bounds of the half-thickness). This entire process relies on the curve growing fast enough that there would still be roots when shifted downwards, yet this is not the case for datasets with very little data points such as Lead-Green. To compensate for this (as curves for many pairings did indeed have roots, just farther out than the maximum absorber widths tested), an arbitrary 'big number', 10^7, was chosen as the bound for the bisection used to find T_{max} (similarly, 0 was used for the T_{min} bound). If even then no root was found, the program merely picks the maximum value within these bounds to give some depiction of the error, even if underrepresented. Because there were only two data points, the curve for Lead-Green plateaued quickly (see Figure 2) and no valid T_{max} existed. Consequently, the program outputted the arbitrary large number of 10^7 (as well as the T_{min} bound of 0), indicating how uncertainty was not legitimately estimable due to the lack of data.

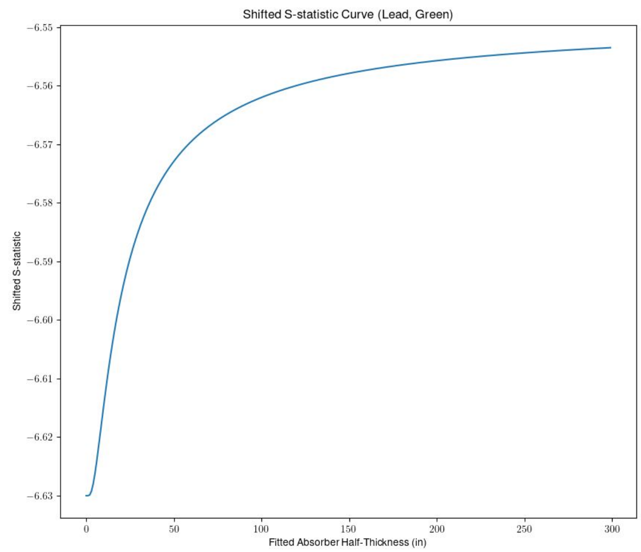

Figure 2: Shifted S-statistic for each half-thickness for the Lead-Green combination. As is visible in the graph, this curve has very large roots, if not none at all.

Plastic was not very absorbent when paired with the green source (with the highest half-thickness of the three absorbers), but the second-most absorbent in the context of the orange source. The discrepancy between its performance in each source is likely due to the general lack of data for the Plastic-Orange pair. Plastic-Orange only has two data points, and as a result the generated fit has similar issues to Lead Green: a large T_{max} as can be seen in Figure 1 and a general inability to accurately determine half-thickness of a material.

Aluminum was more absorbent than plastic (except for the case of the orange source where inaccuracies in determining the plastic half-thickness affected the results) and less absorbent than lead. This is to be expected as aluminum is denser than most common plastics and therefore is more effective at scattering and stopping radiation, yet less dense than lead making it less effective at blocking radiation.

No conclusions can be drawn concerning the absorption capabilities of tissues due to there being only one analyzed trial.

Error for each of the fits could have been affected by physical sources of error in the measurements. Potential physical sources of error include uncertainty in the thickness of each material. Although each material was presented as a certain thickness, there is some error in that measurement. The exact uncertainty is unknown however. Additionally, the Geiger counter itself is likely to experience false positives and negatives leading to further error in the measured values. The exact rate of such false positives and negatives is also unknown as Vernier doesn't provide any such statistic, but given the nature of the sensor, both of these rates are likely relatively low.

The Tissue-Yellow half-thickness is indicative that the yellow radiation source is alpha radiation, as the very low half-thickness (tissues were considered too thin to measure accurately in inches) is reminiscent of how alpha particles are easily stopped.

The green source had a very low half-thickness for lead, a low half-thickness for aluminum, and a moderate one for plastic. It therefore is more likely to be emitting beta radiation as beta radiation can be effectively stopped by aluminum.

Finally, the orange source has significantly larger half-thicknesses for each absorber than the green source, with double the lead half-thickness. The significantly higher overall permeability as well as the large half-thicknesses for plastic and aluminum suggests that the orange source is emitting gamma radiation, as plastic and aluminum are not very effective at blocking gamma radiation.

Conclusion:

Despite errors caused by a lack of data points for specific trials, the overall results matched theoretical expectations. Lead was the most absorbent material, and if one discounts the erroneous Plastic-Orange trial, aluminum was the second-most absorbent, and plastic the least so. This corresponds directly with the theoretical absorption capabilities of each material: lead is the most dense and plastic the least. Additionally we found that the yellow source was emitting alpha radiation, the green emitting beta radiation, and the orange emitting gamma radiation.

As can be seen in Table 4, the fit half-thicknesses were accurate overall: for each combination of source and absorber the S_{min} was less than N-1, where N is the number of datapoints. For some combinations like Lead-Green and Plastic-Orange it was particularly close to N-1, and this is largely due to a lack of data points causing fits to be of poor quality. This is also visible (albeit subjectively) in Figure 1, where the fit line in green is generally close to the recorded line in blue.

Given further resources, the findings within this report could be supported by larger amounts of data since it would allow the generation of more representative models and therefore more accurate conclusions. Further, creating a better programmatic fitting routine, the generated models could be given greater accuracy additionally aiding the conclusions of this report. Such a fitting routine could better optimize for fits with low data counts (like Lead-Green and Plastic-Orange) as well as additionally achieve higher accuracy for the rest.